PASJ: Publ. Astron. Soc. Japan **63**, S657–S668, 2011 November 25

Cross Spectral Calibration of Suzaku, XMM-Newton, and Chandra with PKS 2155−304 as an Activity of IACHEC

Manabu ISHIDA,[1] Masahiro TSUJIMOTO,[1] Takayoshi KOHMURA,[2] Martin STUHLINGER,[3] Michael SMITH,[4] Herman L. MARSHALL,[5] Matteo GUAINAZZI,[4] Kohei KAWAI,[2] and Taiki OGAWA[2]

[1]*The Institute of Space and Astronautical Science/JAXA, 3-1-1 Yoshinodai, Chuo-ku, Sagamihara 252-5210*
ishida@astro.isas.jaxa.jp

[2]*Department of Physics, Kogakuin University, 2665-1 Nakano-cho, Hachioji, Tokyo 192-0015*

[3] *XMM-Newton Science Operations Centre, European Space Astronomy Centre (ESAC), Villafranca, PO Box 50727, 28080 Madrid, Spain*

[4]*European Space Astronomy Centre of the European Space Agency, PO Box 78, Villanueva de la Cañada, E-28691 Madrid, Spain*

[5]*Kavli Institute for Astrophysics and Space Research, Massachusetts Institute of Technology, 77 Massachusetts Ave., Cambridge, MA 02139, USA*

(Received 2011 August 23; accepted 2011 September 11)

Abstract

We report on comparisons of the energy responses of the Suzaku XIS, the Chandra HRC and ACIS with the LETG, and the XMM-Newton MOS and pn using simultaneous data of the BL Lac object PKS 2155−304 taken in 2005, 2006, and 2008. From power-law fits to individual spectra, we have found that the photon index agrees among all instruments within $\simeq 0.1$, and that the resultant hydrogen column density values of the Chandra and XMM-Newton instruments differ from the value for PKS 2155−304 only by $\lesssim 1 \times 10^{20}\,\mathrm{cm}^{-2}$, while that of Suzaku bears a larger systematic error of $4 \times 10^{20}\,\mathrm{cm}^{-2}$, at most. We have carried out flux cross-calibration in seven small segments of energy bands between 0.5 keV and 10 keV. In the bands above 2 keV, the Suzaku fluxes are larger than those of XMM-Newton by $\simeq 20\%$, $\simeq 10\%$, and $\lesssim 5\%$ in 2005, 2006, and 2008, respectively, although the 20% difference in 2005 is still preliminary. The fluxes of the LETG+HRC in 2006 coincide with those of Suzaku below 2 keV. The fluxes of the LETG+ACIS are compared with those of Suzaku and XMM-Newton with the 2008 data, and are systematically larger than those of Suzaku and XMM-Newton by 10%. These results are in general consistent with those presented in one of the precedent papers from International Astronomical Consortium for High Energy Calibration (IACHEC) using G21.5−0.9.

Key words: instrumentation: detectors — X-rays: individual (PKS 2155−304)

1. Introduction

A number of X-ray observatories have been launched since 1970. Simultaneous observation campaigns on the same targets were sometimes organized among them. In addition, the amount of archival data from these observatories has been rapidly growing, and many targets were observed by different observatories at different epochs. In order to investigate the nature of X-ray targets by utilizing a wealth of these data, it has become highly important to cross-calibrate their energy response matrices. In response to this desire, we organized a simultaneous observation campaign of the BL Lac object PKS 2155−304 among three major X-ray observatories: Suzaku (Mitsuda et al. 2007), XMM-Newton (Jansen et al. 2001), and Chandra (O'dell & Weisskopf 1998).

To compare X-ray spectra and resultant physical quantities, it is preferable to choose a point-like source as a calibration target, because we need to care about telescope vignetting in the case of diffuse sources. Although rotation-powered pulsars are advantageous in that they are steady and have a simple power-law spectrum below 10 keV, they are usually buried in an associated diffuse supernova remnant, and suffer heavy interstellar absorption sometimes amounting to $N_{\mathrm{H}} \sim 10^{22}\,\mathrm{cm}^{-2}$, which precludes us from cross-calibrating the effective area below ~ 2 keV.

As described above, there is no ideal calibration source in the sky that is perfect for all the calibration purposes. In practice, we need to combine several different sources with partially ideal characteristics. Beuermann et al. (2006) showed the cross-calibration results at the super soft band (< 0.5 keV) using isolated white dwarfs and neutron stars. Nevalainen et al. (2010) and Tsujimoto et al. (2011), on the other hand, showed results in the hard band (2–8 keV) using relaxed clusters of galaxies and the pulsar-wind nebula associated with G21.5−0.9, respectively. The 0.5–2.0 keV band inbetween is particularly important for cross-calibration purposes, because this is where some challenging calibration effects become most apparent, which includes contamination modeling, and a redistribution of hard band photons into the soft-band. Although the clusters are very bright in this band, especially if they have cool cores, they are extended, and possibly have complicated temperature and spectral structures, which are usually major problems for calibration. The pulsar-wind nebula of G21.5−0.9, on the other hand, does not show intense emission in the 0.5–2.0 keV band due to heavy intervening absorption. The BL Lac object PKS 2155−304 is an ideal target to cover

Table 1. Observation log of PKS 2155−304 with Suzaku, XMM-Newton, and Chandra.

Mission	*ObsID*	Instruments	Observation start	Window	Filter	SCI	Exposure [ks]
Suzaku	700012010	XIS 0,1,2,3	2005-11-30 18:35:59	1/8	—	off	63.9
	101006010	XIS 0,1,2,3	2006-05-01 06:14:32	1/4	—	off	38.6
	102020010	XIS 0,1,3	2007-04-22 12:30:04	1/4	—	on	12.0
	103011010	XIS 0,1,3	2008-05-12 13:42:05	1/4	—	on	23.1
XMM-Newton	0158961301	pn,MOS 1,2	2005-11-30 20:34:03	SW	Medium	—	60.4
	0158961401	pn,MOS 1,2	2006-05-01 12:25:55	SW	Medium	—	64.8
	0411780201	pn,MOS 1,2	2007-04-22 04:07:23	SW	Medium	—	67.9
	0411780301	pn,MOS 1,2	2008-05-12 15:02:34	SW	Medium	—	61.2
Chandra	6923	LETG+HRC	2006-05-01 11:57:39	—	—	—	30.2
	8379	LETG+HRC	2007-04-22 12:25:45	—	—	—	30.1
	9704	LETG+ACIS-S	2008-05-12 13:31:01	—	—	—	29.4

the 0.5–2.0 keV band and beyond for its small intervening absorption, moderate brightness, and a relatively soft spectral shape. Considering these factors, we have conducted a simultaneous observation campaign of PKS 2155−304 among the three major X-ray observatories, Suzaku, XMM-Newton, and Chandra, once per year since 2005. The X-ray spectrum of PKS 2155−304 can be approximated by a simple power law with a photon index of 2.5–2.7, depending upon its intensity; the line-of-sight hydrogen column density is as small as $1.7 \times 10^{20}\,\mathrm{cm}^{-2}$. The source is, however, highly variable. We therefore need simultaneous coverage among the three missions.

This paper is organized as follows. In section 2, we overview the observations of each observatory, including derivations of intersection good-time interval (GTI) files. In section 3, we present the results of spectral analysis on the basis of the intersection GTI files, and compare the spectral parameters and fluxes among the three observatories. We provide summaries of our results in section 4. Throughout the present work, we used XSPEC (Arnaud 1996) version 11.3.2ag as the spectral fitting tool, and all the errors quoted hereafter are at the 90% confidence level, unless otherwise mentioned.

This paper is a summary of the activity of a working group aiming at calibrating the effective areas of different X-ray missions within the framework of the International Astronomical Consortium for High Energy Calibration (IACHEC: Sembay et al. 2010). IACHEC aims to provide standards for high-energy calibration and to supervise cross calibration between different missions. We refer the readers to a website[1] for more details on IACHEC activity.

2. Observations

2.1. Observation Log

In table 1, we summarize the observation log of Suzaku, XMM-Newton, and Chandra for this simultaneous observation campaign from 2005 to 2008. We continued our coordinated observation campaign in 2009, 2010, and 2011, the results of which will be shown elsewhere. We analyzed the data of the instruments that cover the 0.5–2.0 keV band and beyond, which includes the XIS (Koyama et al. 2007) of Suzaku, the EPIC MOS (Turner et al. 2001) and pn (Strüder et al. 2001) cameras of XMM-Newton, and the HRC (Murray et al. 1997) or the ACIS (Burke et al. 1997) with the LETG (Brinkman et al. 1987, 1997; Predehl et al. 1997).

In 2005, Chandra did not participate in the campaign, and we have data only from Suzaku and XMM-Newton. All of the three observatories have taken part in the campaign since 2006. One of the XIS modules, XIS 2, has been unusable since 2006 November 9, probably due to micrometeorite impacts on the CCD chip. We have applied spaced-row charge injection (SCI: Uchiyama et al. 2009) to all XIS modules since 2006 October, to recover the spectral resolution of the XIS. Since PKS 2155−304 is moderately bright, both Suzaku and XMM-Newton CCDs are operated in partial window modes, which are either 1/8 or 1/4 window options in the Suzaku XIS, and Small Window option in the XMM-Newton pn and MOS, in order to reduce the effect of photon pile-up. We do not analyze RGS data of XMM-Newton, since its energy band is limited up to 2 keV, and the cross-calibration between the RGS and the EPIC cameras is presented elsewhere.[2] Chandra has participated in the campaign since 2006 with the grating instrument (LETG), which is free from photon pile-up and telemetry saturation.

2.2. Creation of Intersection GTI Files

As mentioned in section 1, PKS 2155−304 is highly variable, and hence we need to apply an intersection GTI file to the event files for extracting spectra from each instrument. In producing the intersection GTI files, we have first screened the data of each instrument separately.

In extracting Suzaku GTIs, we started with the event files processed with the pipe-line-processing software version 2.0.6.13 in 2005, 2006, and 2007, and with 2.0.6.18 in 2008. Standard data reduction criteria are applied, which include a part for excluding data obtained while the XIS field of view is

[1] ⟨http://web.mit.edu/iachec/⟩.

[2] ⟨http://xmm2.esac.esa.int/docs/documents/CAL-TN-0052.ps.gz⟩.

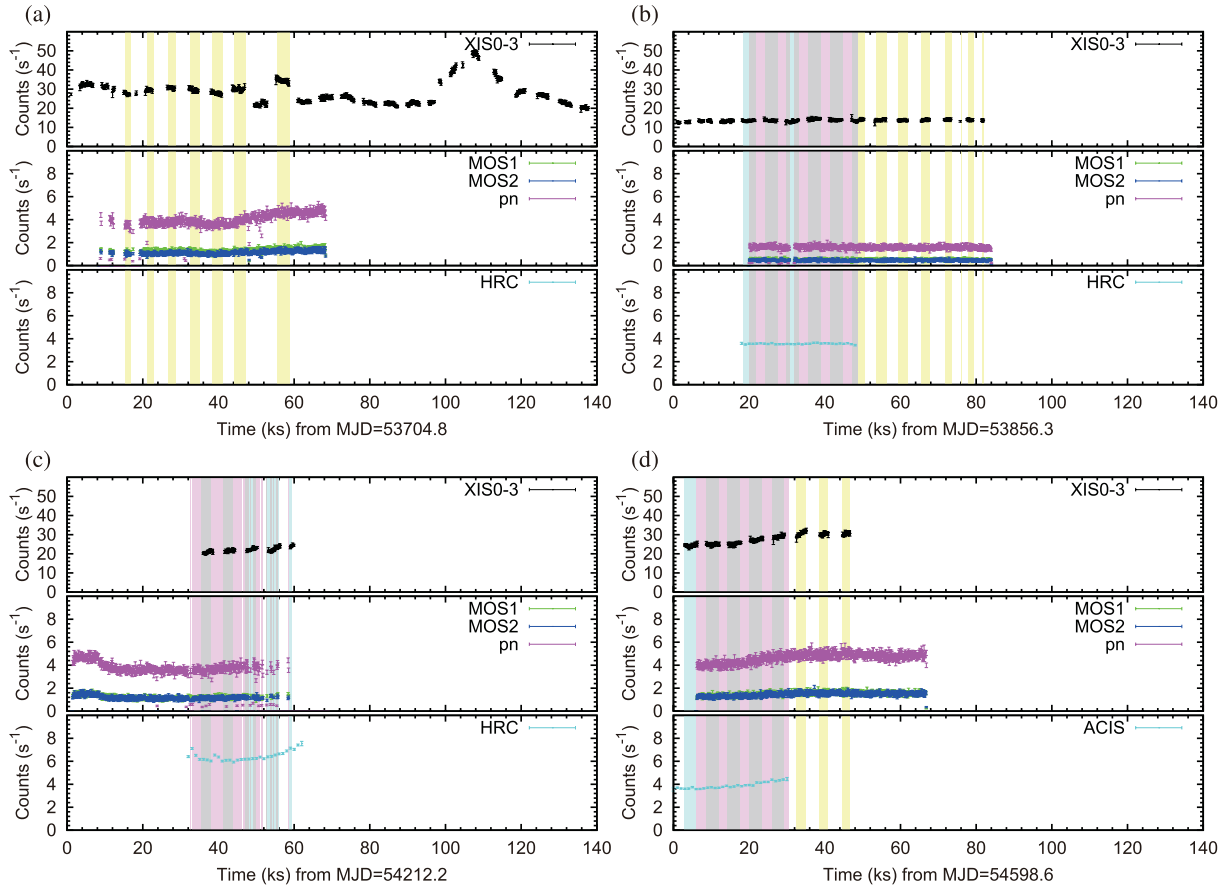

Fig. 1. Light curves of the Suzaku XIS, the XMM-Newton EPIC cameras, and the Chandra HRC and ACIS with the LETG in (a) 2005, (b) 2006, (c) 2007, and (d) 2008. The Suzaku light curves were made by combining all XIS modules at work. We had 4 XIS modules in 2005 and 2006, whereas 3 in 2007 and 2008 (XIS 2 died in 2006 November). The overlap intervals between Suzaku and XMM-Newton, between XMM-Newton and Chandra, and between Chandra and Suzaku are shown with stripes colored in yellow, magenta, and blue, respectively, while those among all three satellites are shown in gray. Note that we did not use the data in 2005 during the intervals 47–52 ks and 60–68 ks, because there was significant optical light leak into the field of view of the XIS 1 and XIS 2. Some data points of the pn appear very close to null counting rate in panels (a) to (c). This is because these data were taken during high background time intervals, whereas no dead time correction was applied.

within 5° or 20° from the night and day Earth rim, respectively, and while the spacecraft passes through the South Atlantic Anomaly. Part of the data suffer telemetry saturation due to sudden flare-up of PKS 2155−304. We have also excluded such time intervals.

The EPIC/MOS and pn data from 2005 to 2007 and those in 2008 were screened with SAS 8.0.0 using the CCF dated on 2008 April 15 and on 2008 November 11, respectively. The HRC+LETG data in 2006 and 2007 were reduced by data-processing software with a version ID of 7.6.7.2 and 7.6.11, respectively. Those of ACIS+LETG were reduced with the software version 7.6.11.6. The GTI files of XMM-Newton and Chandra were created according to the standard data-processing procedure.

The light curves obtained by applying the GTI files thus created are shown in figure 1. For the XMM-Newton data, the source photons were integrated with an annulus with an inner and outer radii of 25″ and 35″ centered on PKS 2155−304 to avoid photon pile-up. The background was not subtracted. Since the imaging capability of the Suzaku XRTs is only moderate, we do not have to care about photon pile-up for a moderate intensity source, like PKS 2155−304. The light curves of the Suzaku XIS were therefore obtained from a circular region with a radius of 4′.33 (= 6.0 mm on the detector surface). The background was not subtracted.

The source was variable both on long and short time scales. It was most intense and variable in 2005, where the combined 4 XIS average counting rate was $\sim 30\,\mathrm{c\,s^{-1}}$, while the source was faintest and nearly constant in 2006, where the combined 4 XIS average counting rate was $\sim 10\,\mathrm{c\,s^{-1}}$. Unexpected optical light intrusion into the XIS 1 and XIS 2 field of view was found to contaminate part of the data in 2005. Accordingly, we removed the data during 47–52 ks and 60–68 ks since the beginning of the Suzaku observation from the intersection GTI file.

Figure 2 gives a summary of the intersection GTIs. In spite of extensive effort, GTIs that encompass all three missions are limited, due to a difficulty to trim the observation window locations of the large observatory-type missions. In general, however, simultaneous coverages between any two missions were longer than 15 ks. Hence, we decided to

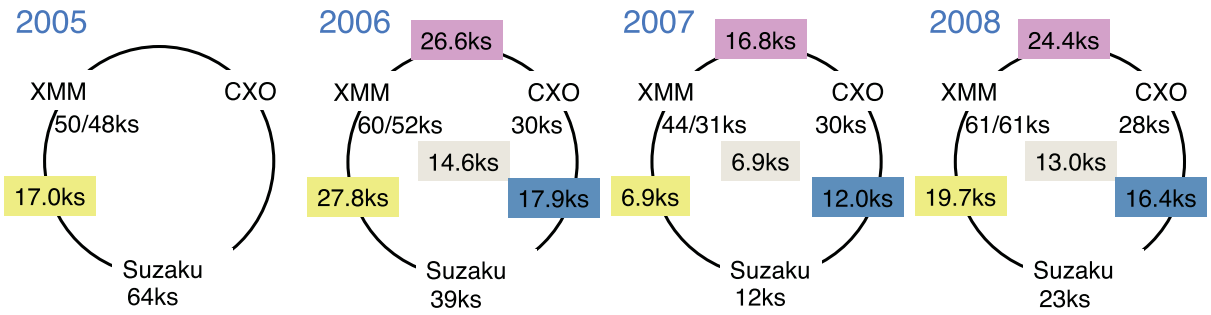

Fig. 2. Summary of the intersection GTIs. The exposure times of each satellite are those after the data screening. For XMM-Newton, the exposure times of the MOS and the pn are shown separately, delineated with a slash. Background color assignment of the intersection exposure times are identical with that in figure 1.

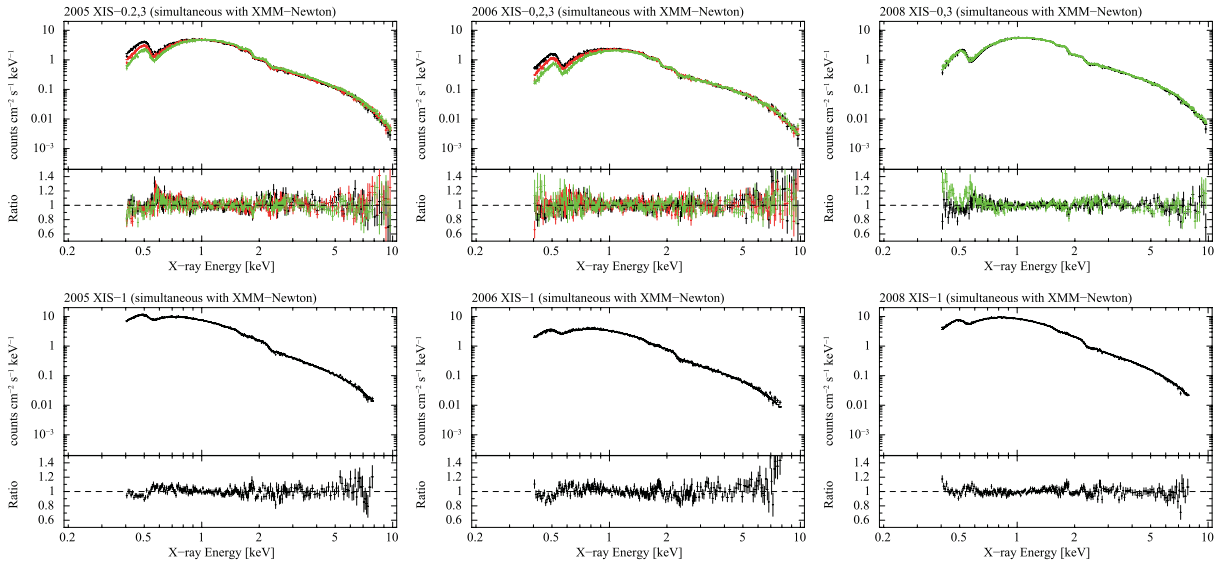

Fig. 3. Suzaku XIS spectra taken simultaneously with XMM-Newton, together with the best-fit power-law models and the fit residuals. The figures are arranged in chronological order from left to right. The upper panels collect the spectra from the FI modules, where XIS 0, XIS 2, and XIS 3 are represented with black, red, and green, respectively, while the lower panels show the spectra of the BI module (XIS 1). Note that we only had two FI modules (XIS 0 and XIS 3) in 2008 (see subsection 2.1).

cross-calibrate the spectral parameters between the pairs of missions. Even with this treatment, the coverage of the 2007 data was not sufficient for detailed spectral analysis. We therefore carried out cross-calibration analysis with the data taken in 2005, 2006, and 2008.

3. Analysis

3.1. Extraction of Spectra

Applying the intersection GTI files described in section 2, we created spectra from one observatory that were simultaneous with the other two. Extraction of the Suzaku spectra was carried out with HEASOFT 6.10 and CALDB dated on 2010 July 30 for both the XIS and the XRT. We accumulated photons with the ASCA grades 0, 2, 3, 4, and 6. We applied a circular integration region with a radius of 4′.33 centered on the source, while the background photons were accumulated from an annulus region out of the source integration region with an outer radius of 6′. Parts of the source and background integration regions were out of the windowed area. This effect was corrected when we created a response file. The XIS spectra simultaneous with those of XMM-Newton and Chandra are shown in figures 3 and 4, respectively.

The EPIC MOS/pn analysis was carried out with SAS version 10.0.2 using CCF as of 2010 August 1. The tasks EMPROC and EPPROC were used to generate calibrated event lists. For spectra integration, we accepted photons with pixel patterns of 0–12 and 0–4 for the MOS and the pn, respectively. We employed a circular region with a radius of 60″ for source photon integration of both the MOS and the pn. In order to avoid photon pile-up, however, the central region of the images are masked. The excluded regions are central circular areas with a radius of 12.″5, 7.″5, and 15″ for the MOS in 2005, 2006, and 2008, respectively, while 10″, 5″, and 10″ for the pn in 2005, 2006, and 2008, respectively. The background photons were collected from source-free regions. The MOS

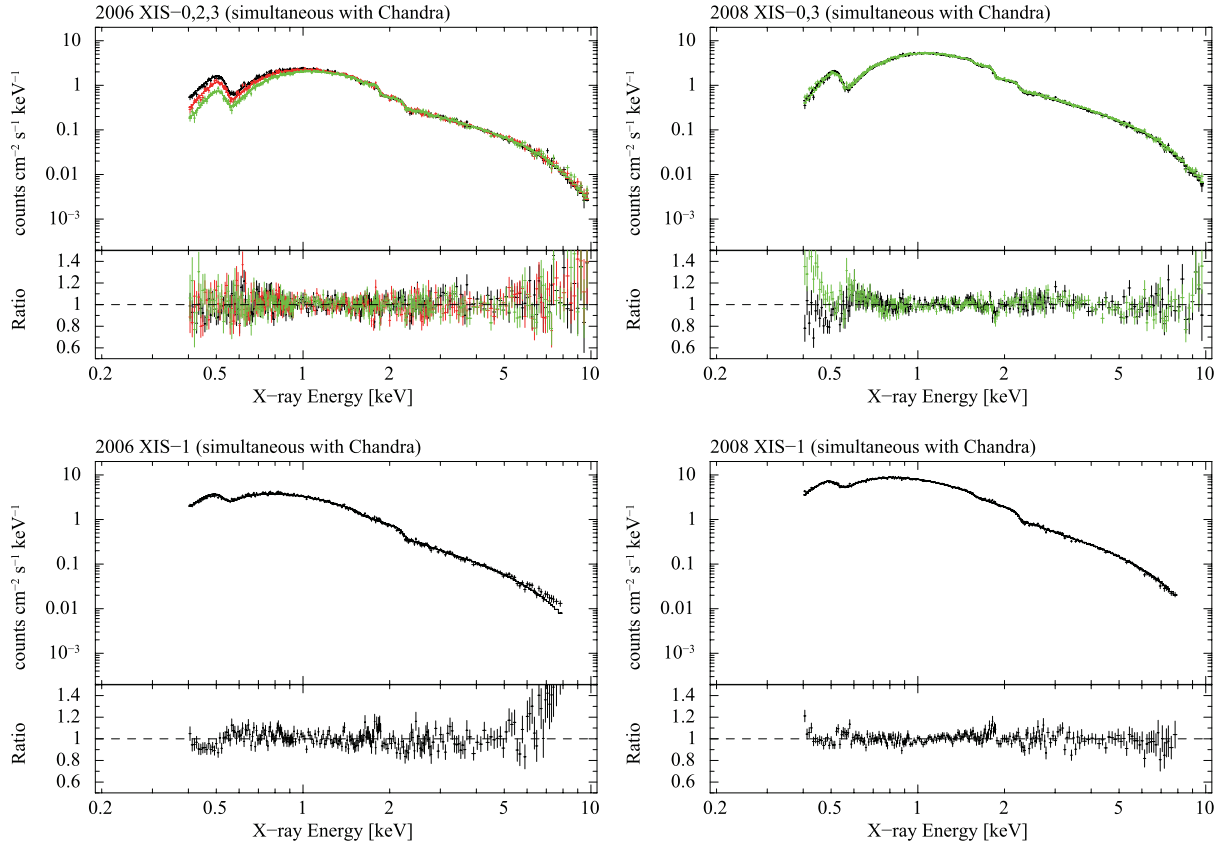

Fig. 4. Suzaku XIS spectra taken simultaneously with Chandra, together with the best-fit power-law models and the fit residuals. The figures are arranged in chronological order from left to right. The upper panels collect the spectra from the FI modules, where XIS 0, XIS 2, and XIS 3 are represented with black, red, and green, respectively, while the lower panels show the spectra of the BI module (XIS 1). Note that we only have two FI modules (XIS 0 and XIS 3) in 2008 (see subsection 2.1).

and pn spectra taken simultaneously with Suzaku and Chandra are shown in figures 5 and 6, respectively.

The Chandra data reduction and spectral extraction were performed with CIAO version 4.2 and CALDB version 4.2.2. We followed the CIAO analysis guides[3] using the standard parameter settings for event filtering, as well as source and background extraction masks. The spectra of Chandra simultaneous along with those of XMM-Newton and Suzaku are shown in figure 7.

3.2. Procedure of Spectral Fitting

Figures 3 through 7 show the spectra of Suzaku, XMM-Newton, and Chandra taken simultaneously with one of the other two observatories, with the best-fit power-law model convolved with a photoelectric absorption. In the present work, we adopted the model PEGPWRLW in XSPEC as the power-law model, in which we set the flux in the 2–10 keV band as the model normalization. There is a report indicating that the X-ray spectrum of PKS 2155−304 can be better described with a broken-power law with a spectral break at $E = 3.5^{+0.5}_{-0.6}$ keV in a low-luminosity state (Foschini et al. 2008). Hence, we first tried to fit the 2006 Suzaku spectra, when the source was the faintest in our dataset, with a broken power law. However, we obtained only an upper limit of < 0.7 keV for the break energy; the data are consistent with no break. We therefore conclude that the spectral break of PKS 2155−304 is not significant in our dataset, and hereafter adopt the simple power-law model (PEGPWRLW) throughout this paper.

We carried out fits to the spectra of the Suzaku Front-Illuminated (FI) CCDs (XIS 0, 2, and 3) in the 0.4–10 keV bands. For the Back-Illuminated (BI) CCD (XIS 1) data, on the other hand, we truncated the spectra at 8 keV in the high-energy end. This is because BI spectra sometimes show excess in this energy band caused by cosmic-ray electrons, whose energy is on the order of $\sim$MeV (Anada et al. 2008). Since this background component is variable, and moreover is not uniform over the detector aperture, the background in this energy band is sometimes highly uncertain (see the BI spectra close to 8 keV in figure 3 and figure 4). In fitting the FI spectra, we introduced a normalization constant to the power-law component, in order to correct for any slight normalization difference among the three FI modules of the XIS. We fixed constant of the XIS 0 at 1.0, and floated the other FI modules. It is known that there is a gain uncertainty in the Suzaku XIS (Koyama et al. 2007; Yamaguchi et al. 2008; Bamba et al. 2008). This gain uncertainty can be resolved by properly introducing an offset of

[3] ⟨http://cxc.harvard.edu/ciao/guides/gspec_acisletg.html⟩ and ⟨http://cxc.harvard.edu/ciao/guides/gspec_hrcsletg.html⟩ for ACIS+LETG and HRC+LETG, respectively.

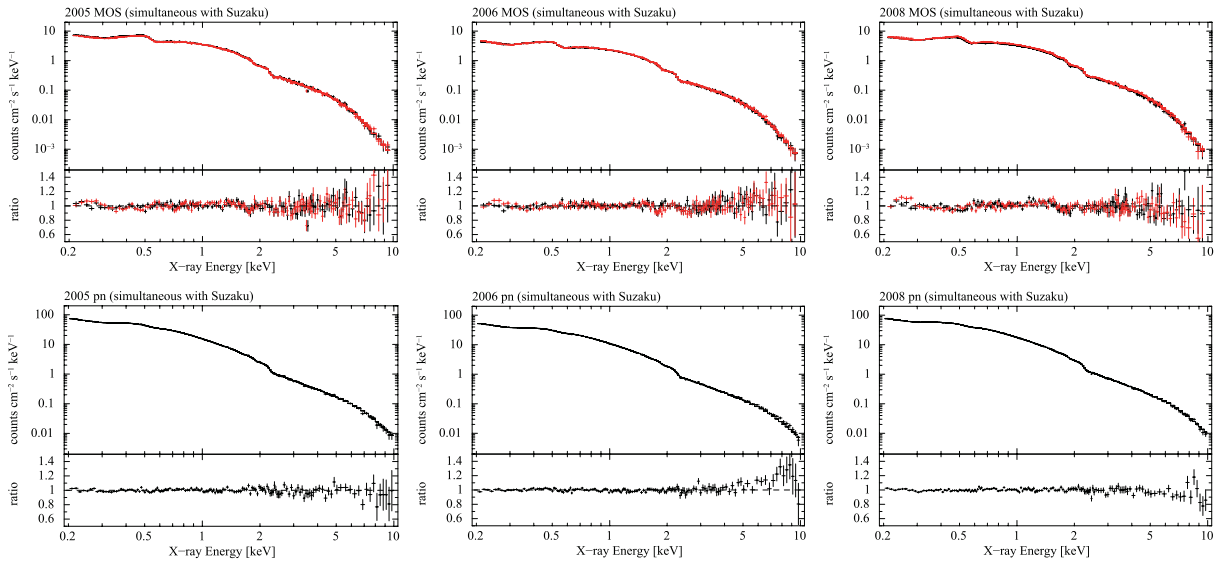

Fig. 5. XMM-Newton EPIC spectra taken simultaneously with Suzaku, together with the best-fit power-law models and the fit residuals. The figures are arranged in chronological order from left to right. The upper panels collect the spectra from the MOS, where MOS 1 and MOS 2 are represented with black and red, respectively, while the lower panels show the spectra of the pn.

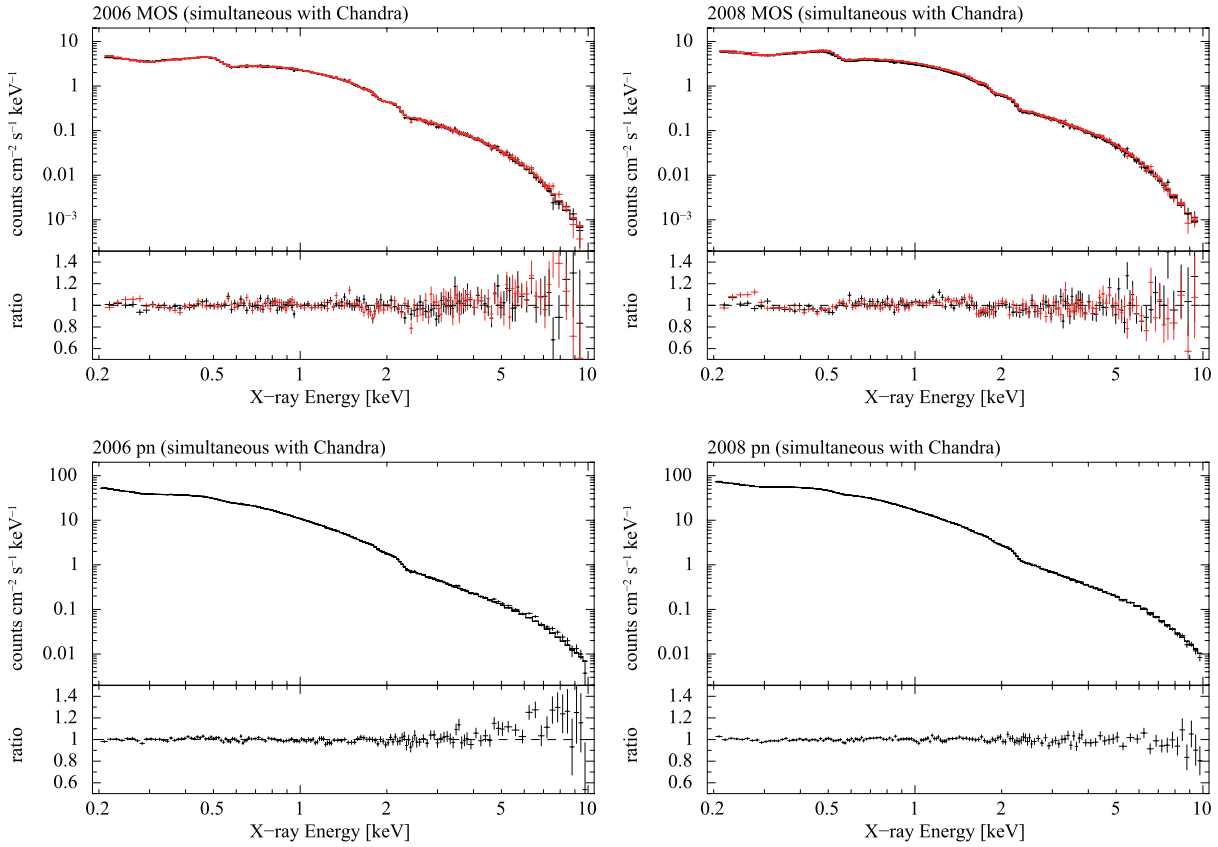

Fig. 6. XMM-Newton EPIC spectra taken simultaneously with Chandra, together with the best-fit power-law models and the fit residuals. The figures are arranged in chronological order from left to right. The upper panels collect the spectra from the MOS, where MOS 1 and MOS 2 are represented with black and red, respectively, while the lower panels show the spectra of the pn.

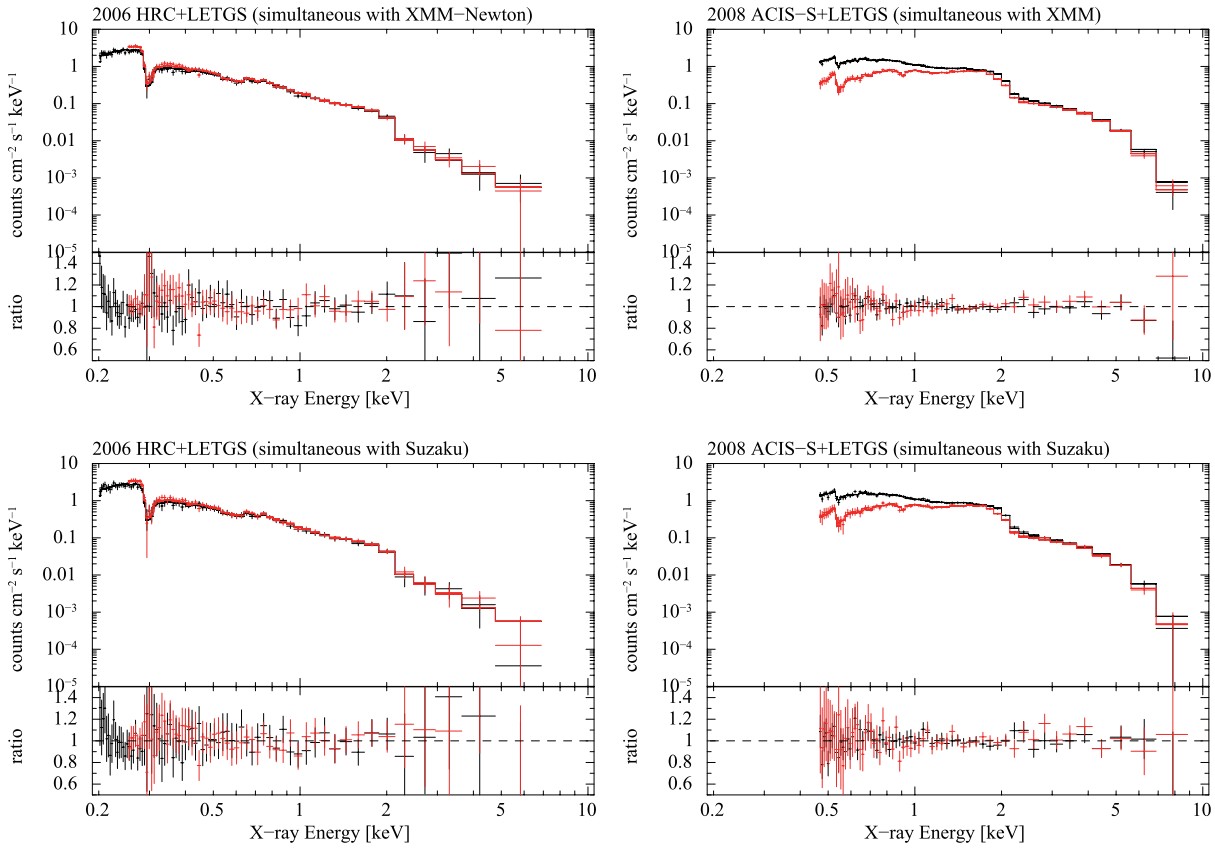

Fig. 7. Spectra of the Chandra HRC+LETG in 2006 and ACIS-S+LETGS in 2008 (± 1 order), together with the best-fit power-law models and the fit residuals. The upper and lower panels show the spectra simultaneous with XMM-Newton and Suzaku, respectively. The +1 order and −1 order data are shown with black and red, respectively.

PH channels, which amounts to $\lesssim$10 eV. Since the gain offset is different among the four XIS modules, we first fitted a power-law model undergoing photoelectric absorption to each XIS spectrum separately in the 0.4–0.7 keV band, and obtained the best gain offset, while referring to the instrumental oxygen K-edge. By fixing them at their best-fit values, we then performed fits to evaluate the physical parameters.

In the spectral fits of XMM-Newton, we adopted the standard 0.2–10 keV band for both MOS and pn. We fitted the MOS and pn spectra separately. In fitting the spectra of the two MOS modules, we introduced a normalization constant, as we did for the Suzaku XIS. We fixed the constant of the MOS 1 at 1.0, and floated that of the MOS2.

In an analysis of the Chandra spectra, we adopted an energy band of 0.45–9 keV for the ACIS+LETG, and fitted the model to the combined ± 1 orders. For the HRC+LETG, in order to avoid chip gaps, we used energy bands of 0.206–7 keV and 0.252–7 keV for the positive and negative order spectra, respectively; the ± 1 order spectra were fitted simultaneously. In fitting the data, no additional normalization constant was introduced either for the HRC or ACIS spectra.

3.3. Comparison of Spectral Parameters

In table 2 we summarize the best-fit parameters of all simultaneous spectra in 2005, 2006, and 2008 with the PEGPWRLW model overlaid with the interstellar photoelectric absorption.

The table contains normalization constant factors, line-of-sight hydrogen column densities, photon indices, and normalizations of the PEGPWRLW model, the gain offsets, and the slopes of the response matrices. The normalization constant factors apply for the MOS and the XIS FI, where they are fixed at unity for the MOS 1 and the XIS 0. The hydrogen column densities were measured in units of 10^{20} cm^{-2}. We adopted Anders and Grevesse (1989) as a reference of the solar abundance, and the BCMC model as representing the cross section of the photoelectric absorption (Bałucińska-Church & McCammon 1992; Yan et al. 1998). The normalizations of the PEGPWRLW model were chosen to be intrinsic (unabsorbed) fluxes in the 2–10 keV band. The offset corrections were applied only to the XIS.

In figure 8, we show confidence contours of all simultaneous pairs in 2005, 2006, and 2008 in the plane of $N_{\rm H}$ versus the photon index. The dotted horizontal lines $N_{\rm H} = 1.7 \times 10^{20}$ cm^{-2} indicate the line-of-sight hydrogen column density to PKS 2155−304 based on Dickey and Lockman (1990). The value was obtained through the tool "nH" supplied by NASA/GSFC.[4]

The left three panels (a), (d), and (g) compare the spectral parameters of XMM-Newton and Suzaku in 2008, 2006, and 2005, respectively. The difference in the photon index between

[4] ⟨http://heasarc.gsfc.nasa.gov/cgi-bin/Tools/w3nh/w3nh.pl⟩.

Table 2. Best-fit parameters of the simultaneous spectra in 2005, 2006, 2008.

Detector	Constant	$N_{\rm H}$*	$\Gamma^{\dagger}$	$A^{\ddagger}$	Offset§	Slope‖	χ^2_ν (d.o.f)
2005 XMM-Newton-Suzaku							
MOS 1	1.0 (fix)	1.38 ± 0.11	2.634 ± 0.011	37.9 ± 0.4	—	—	1.48 (280)
MOS 2	1.036 ± 0.007						
pn	—	1.27 ± 0.06	2.678 ± 0.008	36.4 ± 0.4	—	—	1.41 (145)
XIS 0	1.0 (fix)	3.41 ± 0.26	2.689 ± 0.010	41.6 ± 0.4	-14.1 (fix)	1.0 (fix)	1.42 (676)
XIS 2	0.957 ± 0.007				-11.4 (fix)	1.0 (fix)	
XIS 3	1.053 ± 0.008				-11.1 (fix)	1.0 (fix)	
XIS 1	—	5.81 ± 0.32	2.720 ± 0.017	42.5 ± 0.6	-11.8 (fix)	1.0 (fix)	1.78 (216)
Reference model#		1.70	2.679	39.625			
2006 XMM-Newton-Suzaku							
MOS 1	1.0 (fix)	0.63 ± 0.10	2.540 ± 0.010	17.1 ± 0.2	—	—	1.14 (280)
MOS 2	1.033 ± 0.007						
pn	—	0.93 ± 0.05	2.597 ± 0.007	16.5 ± 0.1	—	—	1.51 (145)
XIS 0	1.0 (fix)	1.27 ± 0.34	2.521 ± 0.012	18.4 ± 0.2	-1.3 (fix)	1.0 (fix)	1.13 (676)
XIS 2	1.018 ± 0.010				$+1.2$ (fix)	1.0 (fix)	
XIS 3	1.032 ± 0.010				$+4.9$ (fix)	1.0 (fix)	
XIS 1	—	4.02 ± 0.43	2.570 ± 0.021	18.7 ± 0.3	-12.0 (fix)	1.0 (fix)	1.71 (216)
2006 Chandra-XMM-Newton							
LETG+HRC	—	1.56 ± 0.17	2.671 ± 0.050	15.7 ± 1.2	—	—	0.55 (131)
MOS 1	1.0 (fix)	0.62 ± 0.10	2.551 ± 0.010	16.8 ± 0.2	—	—	1.19 (280)
MOS 2	1.033 ± 0.007						
pn	—	0.96 ± 0.05	2.617 ± 0.007	15.9 ± 0.2	—	—	1.42 (145)
2006 Suzaku-Chandra							
XIS 0	1.0 (fix)	1.01 ± 0.37	2.541 ± 0.013	17.5 ± 0.2	-2.3 (fix)	1.0 (fix)	1.01 (676)
XIS 2	1.025 ± 0.011				-1.5 (fix)	1.0 (fix)	
XIS 3	1.052 ± 0.011				-7.0 (fix)	1.0 (fix)	
XIS 1	—	$4.45^{+0.61}_{-0.42}$	$2.620^{+0.016}_{-0.017}$	$17.6^{+0.21}_{-0.22}$	-13.0 (fix)	1.0 (fix)	1.65 (216)
LETG+HRC	—	1.52 ± 0.22	2.665 ± 0.065	15.8 ± 1.6	—	—	0.39 (131)
Reference model#		1.70	2.5883	17.01			
2008 XMM-Newton-Suzaku							
MOS 1	1.0 (fix)	1.59 ± 0.12	2.584 ± 0.010	47.3 ± 0.5	—	—	1.88 (280)
MOS 2	1.065 ± 0.007						
pn	—	1.47 ± 0.05	2.635 ± 0.006	45.9 ± 0.4	—	—	1.36 (145)
XIS 0	1.0 (fix)	1.17 ± 0.30	2.606 ± 0.010	45.8 ± 0.3	$+12.2$ (fix)	1.0 (fix)	1.55 (450)
XIS 3	1.033 ± 0.006				-4.2 (fix)	1.0 (fix)	
XIS 1	—	3.32 ± 0.29	2.624 ± 0.013	47.7 ± 0.5	-13.5 (fix)	1.0 (fix)	1.62 (216)
2008 Chandra-XMM-Newton							
LETG+ACIS	—	1.06 ± 0.68	2.607 ± 0.030	48.4 ± 1.1	—	—	0.67 (123)
MOS 1	1.0 (fix)	1.43 ± 0.11	2.581 ± 0.009	44.9 ± 0.5	—	—	1.91 (280)
MOS 2	1.068 ± 0.007						
pn	—	1.43 ± 0.05	2.635 ± 0.006	43.5 ± 0.3	—	—	1.05 (145)
2008 Suzaku-Chandra							
XIS 0	1.0 (fix)	0.96 ± 0.34	2.603 ± 0.011	42.4 ± 0.4	$+9.4$ (fix)	1.0 (fix)	1.45 (450)
XIS 3	1.024 ± 0.007				$+5.2$ (fix)	1.0 (fix)	
XIS 1	—	3.05 ± 0.33	2.622 ± 0.015	44.4 ± 0.5	-15.5 (fix)	1.0 (fix)	1.49 (216)
LETG+ACIS	—	0.71 (<1.73)	2.606 ± 0.045	47.9 ± 1.6	—	—	0.61 (123)
Reference model#		1.70	2.6095	45.85			

* Hydrogen column density in units of $10^{20}\,{\rm cm}^{-2}$.
† Photon index of the PEGPWRLW model.
‡ Normalization of the PEGPWRLW model, which is set to the flux in the 2–10 keV band in units of $10^{-12}\,{\rm erg\,cm^{-2}\,s^{-1}}$.
§ Energy offset of the response matrix in units of eV (only for Suzaku).
‖ Correction factor of the proportional constant of the response gain (only for Suzaku).
#Average spectral parameters to be used for the flux calibration (subsection 3.4).

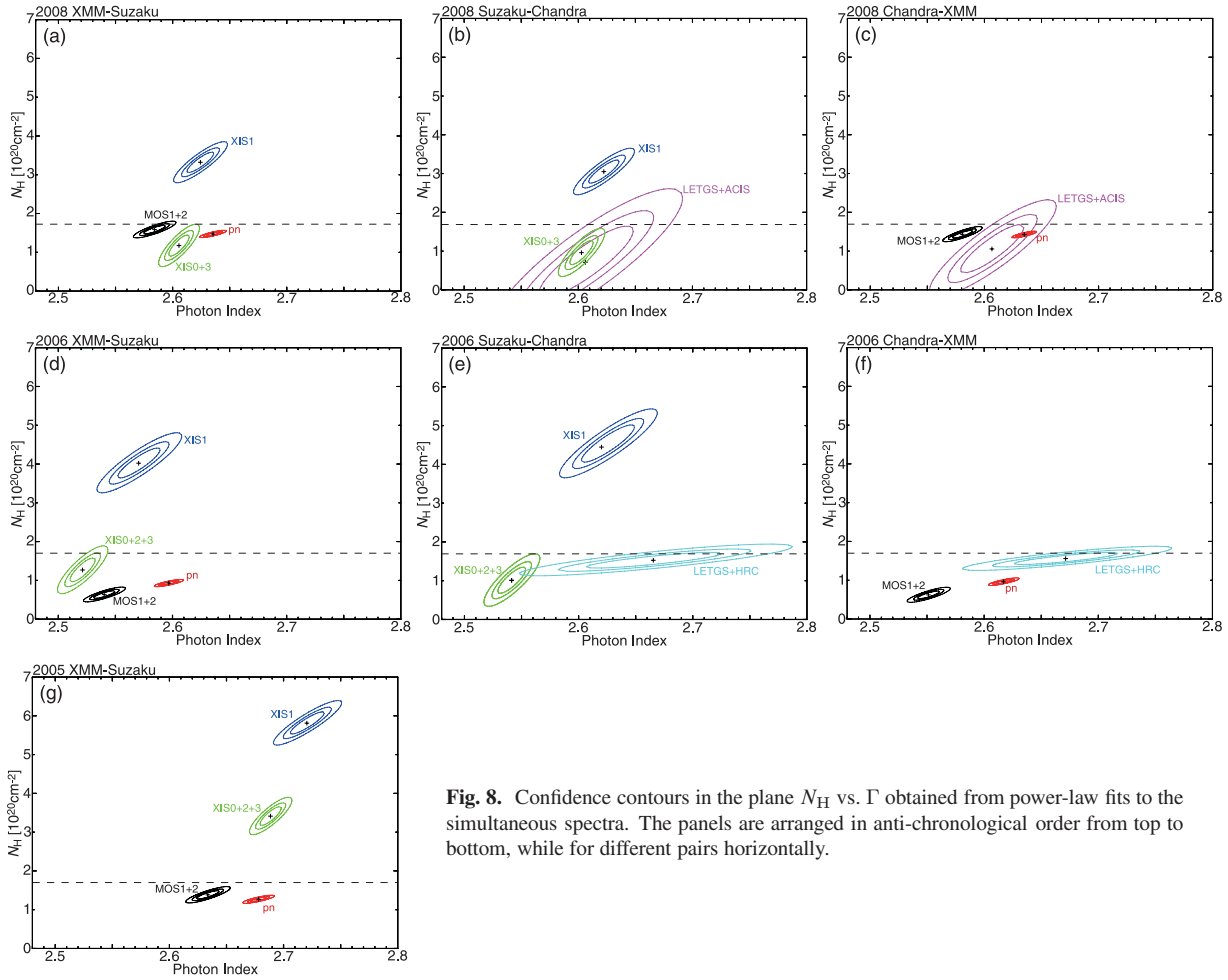

Fig. 8. Confidence contours in the plane $N_{\rm H}$ vs. Γ obtained from power-law fits to the simultaneous spectra. The panels are arranged in anti-chronological order from top to bottom, while for different pairs horizontally.

Suzaku and XMM-Newton is $\lesssim 0.1$, in general. The internal calibration uncertainty of the photon index is as small as $\lesssim 0.05$ between the XIS FI and the BI, and between the MOS and the pn. The deviation of the hydrogen column density from that to PKS 2155−304 is relatively small for the XMM-Newton instruments, which is $N_{\rm H} \lesssim 3 \times 10^{19}\,{\rm cm}^{-2}$, whereas that of Suzaku is at most $4 \times 10^{20}\,{\rm cm}^{-2}$. The latter is basically due to the calibration uncertainty concerning the amount of contaminant on the XIS aperture window filters. According to subsection 7.7 of the Suzaku technical description,[5] there remains a random fluctuation of the measured carbon column density around the calibration curves, which amounts to $5 \times 10^{17}\,{\rm C\,cm}^{-2}$, at most. Since [C/H] $= 3.63 \times 10^{-4}$ in the abundance table of Anders and Grevesse (1989), this uncertainty of the carbon column density could result in an error of $N_{\rm H}$ as much as $\lesssim 1.4 \times 10^{21}\,{\rm cm}^{-2}$ in our spectral fitting. The real systematic errors of $N_{\rm H}$ shown in figure 8 are well within this range. The large deviation of $N_{\rm H}$ of the Suzaku XIS requires further effort for improving the contamination analysis. The XIS team has put effort on tuning the contamination model by, for example, introducing a time variation of the contaminant chemical composition.

The spectral parameters of the LETG+ACIS are compared with those of Suzaku and XMM-Newton in panels (b) and (c). The observation was carried out in 2008. Although the error regions are larger than those of Suzaku and XMM-Newton, the photon index of the LETG+ACIS matches very well with that of Suzaku and XMM-Newton within 0.02. The deviation of the hydrogen column density from the one to PKS 2155−304 is on the order of $1 \times 10^{20}\,{\rm cm}^{-2}$.

The same comparison of the LETG+HRC is made in the panels (e) and (f), which are based on the 2006 data. Although the error regions are even elongated, the photon index determined with the LETG+HRC seems to be larger than those with Suzaku and XMM-Newton by 0.05–0.1. The hydrogen column density is, on the other hand, calibrated very well, and its deviation from that to PKS 2155−304 is $N_{\rm H} \lesssim 2 \times 10^{19}\,{\rm cm}^{-2}$.

A spectral parameter comparison among various ongoing missions was presented in another IACHEC paper (Tsujimoto et al. 2011) using the compact SNR G21.5−0.9, which has a non-thermal power-law type spectrum with a photon index of 1.7–1.9, undergoing heavy photoelectric absorption ($N_{\rm H} \sim 3 \times 10^{22}\,{\rm cm}^{-2}$). Since they used ACIS-S3 data without grating for Chandra, we can compare our results with theirs on Suzaku and XMM-Newton. The photon index of the Suzaku and XMM-Newton instruments concentrates in the ranges of 1.90–1.92 and 1.76–1.84, respectively, with a typical statistical error of ± 0.02 for both. This result is not completely

[5] ⟨http://www.astro.isas.jaxa.jp/suzaku/doc/suzaku_td/⟩.

the same as our results in that the internal inconsistency of the XMM-Newton photon index obtained by Tsujimoto et al. (2011) seems to be as large as the inter-mission inconsistency of ~ 0.1 (see our results shown in figures 8a, 8d, 8g). In general, however, the photon index difference between the Suzaku and XMM-Newton instruments is on the order of 0.1 both in Tsujimoto et al. (2011) and this paper. Tsujimoto et al. (2011) used the XMM-Newton data taken in 2000 April, whereas Suzaku data were taken in 2009 October. Our 2008 analysis on Suzaku XIS, closest in time to Tsujimoto et al. (2011), shows that the photon index difference between the XIS 0, 3 and the XIS 1 is 0.02 (typical statistical error ± 0.01), which is consistent with Tsujimoto et al. (2011) (table 2). The photon index difference between the MOS 1, 2 and the pn, on the other hand, is $\simeq 0.05$ from our analyses in 2005, 2006, and 2008. Although this amount is similar to that of Tsujimoto et al. (2011), the pn shows a larger photon index in our analysis, whereas it is smallest in Tsujimoto et al. (2011).

3.4. Comparison of Energy-Resolved Fluxes

In science papers, fluxes are usually derived in a relatively wide energy band, such as 2–10 keV. Such a wide energy band, however, bears potential danger to bring a large systematic error to the resultant flux. This is mainly because the quantum efficiency or the effective area of X-ray instruments is not generally uniform over their sensitive energy bands. In such a case, the continuum shape parameters, such as the photon index, is determined by weighing data points where the detector has a relatively high efficiency. If the spectral calibration of the high-efficiency band is not perfect, which is usually the case, the systematic error propagates to a low-efficiency energy band.

In order to avoid such a systematic error, we have decided to compare the fluxes in small segments of the energy bandpass. In this paper, we adopt the following seven energy bands for flux comparisons: 0.5–1.0keV, 1.0–1.5 keV, 1.5–2.0 keV, 2.0–3.0 keV, 3.0–4.0 keV, 4.0–6.0 keV, and 6.0–10.0 keV. Although we have assigned wider energy spans for higher energy bands, the available numbers of photons in higher energy bands are much smaller than in the lower energy bands, due to the steep spectral slope $\Gamma = 2.5$–2.7 of PKS 2155−304. Nevertheless, even in 2006 when the source is the weakest, Suzaku XIS 1 (BI) simultaneous with Chandra (17.9 ks) still retains ~ 1000 photons in the 6–8 keV band, and the two MOS units simultaneous with Chandra (26.6 ks) have ~ 770 photons in the 6–10 keV band, both after background subtraction.

In evaluating the flux in each of the seven energy bands, we first ignored the data points out of the energy band of interest. We then fitted a power-law model undergoing photoelectric absorption to the spectra. In this fitting, the hydrogen column density, the photon index, and its normalization were all set free to vary. Floating the hydrogen column density is of particular importance to obtain acceptable fits in the lower energy band below 1.5 keV. In calculating the flux, we used the FLUX command in XSPEC. This means that we calculated the observed fluxes, and the extinction due to the photoelectric absorption was not removed.

The results are shown in figure 9 as ratios to a reference model. The reference models are again a power law undergoing photoelectric absorption. The photon index and the normalization are an average of the best-fit values listed in table 2 for each year separately, which are tabulated in the row labeled "Reference model". The hydrogen column density is fixed at the value to PKS 2155−304 ($= 1.7 \times 10^{20}\,\mathrm{cm}^{-2}$).

Panels (a), (d), and (g) compare the energy-resolved fluxes of Suzaku and XMM-Newton. The fluxes from the FI modules of the XIS and MOS are taken from XIS 0 and MOS 1, respectively. It is clear that the Suzaku fluxes in 2005 and 2006 are larger that those of XMM-Newton above ~ 2 keV by $\simeq 20\%$ and $\simeq 10\%$, respectively. The flux difference in 2008 is smaller than in 2005 and 2006, which is $\lesssim 5\%$. Note that the flux difference of $\simeq 20\%$ in 2005 is somewhat large. This result, however, should be treated as being preliminary, considering that the observation in 2005 was carried out with the 1/8 window option in which the field of view of each XIS instrument was limited to a square with $2'.22 \times 17'.8$. Although PKS 2155−304 is placed at the center of this field of view, the Suzaku pointing direction wobbles by as much as $50''$ due to thermal distortion of the optical bench, which changes associated with the spacecraft orbital motion (Uchiyama et al. 2008). In addition, there still remains uncertainty of the point-spread function of the XRT[6] amounting to $\sim 10\%$ within the central $2'$ region in diameter. These effects could result in a flux error on the order of $\sim 10\%$. We need to further carefully study the point-spread function before finalizing the Suzaku fluxes of PKS 2155−304 in 2005.

The flux difference between Suzaku and XMM-Newton became smaller in the lower energy bands in 2005. This was, however, due to the larger hydrogen column densities of the XIS (see table 2 and figure 8g), associated with the calibration error of molecular contamination of the optical blocking filters (see subsection 3.3). Were it not for the flux difference of 20% above 2 keV, there would have appeared flux a discrepancy in the lower energy bands instead.

Panels (b) and (c) show the energy-resolved fluxes of the LETG+ACIS to those of Suzaku and XMM-Newton with the 2008 data. As described above, the fluxes of Suzaku and XMM-Newton are consistent within $\simeq 5\%$ in 2008 [panel (a)]. Compared with them, the fluxes of the LETG+ACIS are systematically larger by $\simeq 10\%$.

Panels (e) and (f) show the energy-resolved fluxes of the LETG+HRC to those of Suzaku and XMM-Newton with the 2006 data. Due to the statistical limitation, the fluxes of the LETG+HRC above 2 keV are not useful. Below 2 keV, the LETG+HRC fluxes seem to be more consistent with those of Suzaku.

Finally, we compare our results on the flux cross calibration between Suzaku and XMM-Newton with those of Tsujimoto et al. (2011), who derived the 2–8 keV intrinsic flux from a power-law fit to individual spectra of G21.5−0.9. According to them, the flux of the pn is 5.07, whereas that of MOS 1 and 2 are 5.47 and 5.37, respectively, in units of $10^{-11}\,\mathrm{erg\,cm^{-2}\,s^{-1}}$. The average MOS flux is larger than that of the pn by 7%. From our analysis, on the other hand, the fluxes of the MOS and the pn agree within a few percent. The fluxes of the XIS 0, 3 (FI) and XIS 1 (BI) are 5.62, 5.66, and 5.73, respectively,

[6] ⟨http://www.astro.isas.jaxa.jp/suzaku/doc/suzaku_td/⟩.

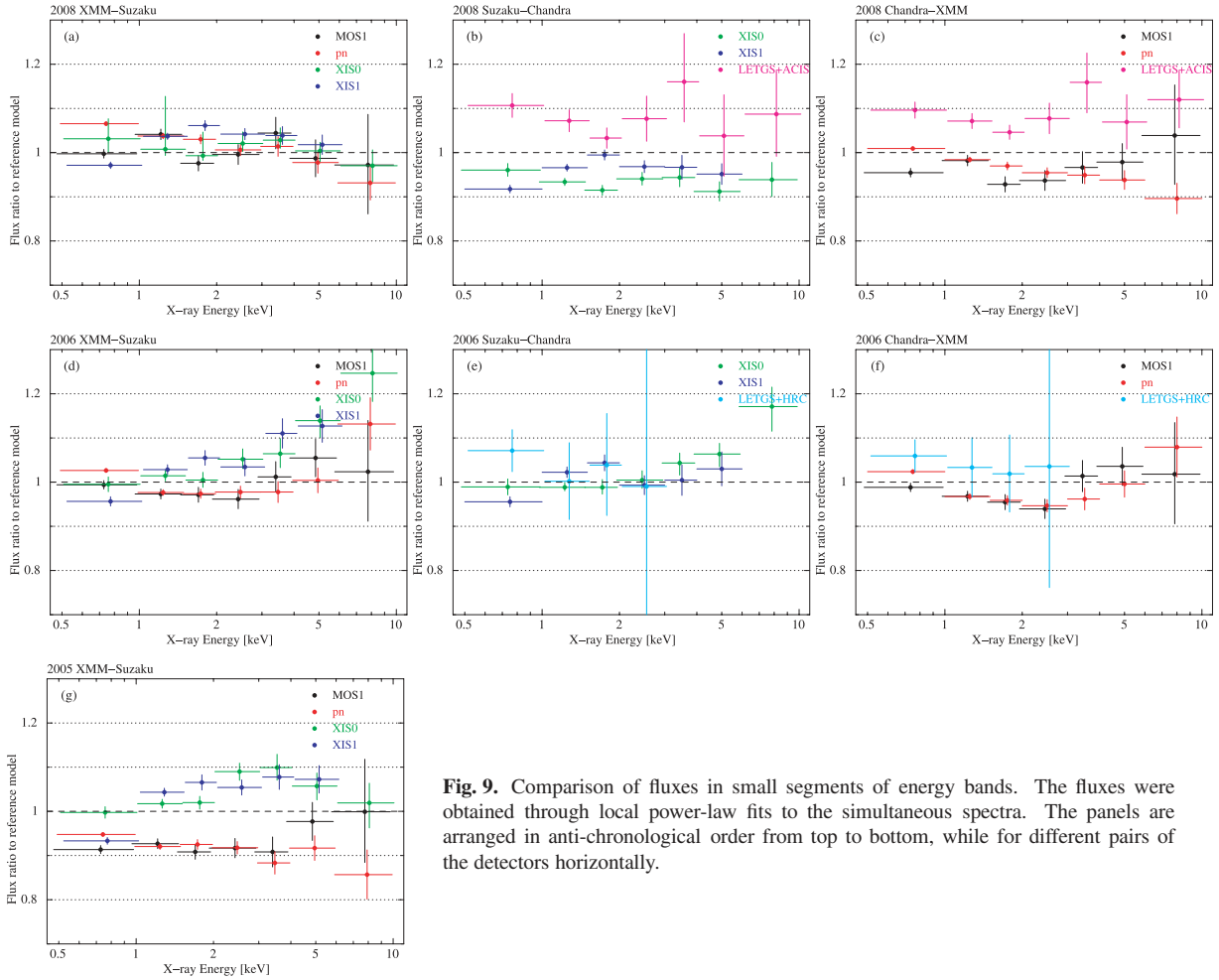

Fig. 9. Comparison of fluxes in small segments of energy bands. The fluxes were obtained through local power-law fits to the simultaneous spectra. The panels are arranged in anti-chronological order from top to bottom, while for different pairs of the detectors horizontally.

in the same units. Hence, the average FI flux and the BI flux are larger than that of the pn by 11% and 13%, respectively. These systematically larger fluxes of Suzaku instruments than the XMM-Newton ones by several to some 10% is qualitatively in agreement with our results. Note again that the XMM-Newton data were taken in 2000 April, while those of Suzaku were in 2009 October in Tsujimoto et al. (2011).

4. Conclusion

We have compared the energy responses of instruments onboard Suzaku (XIS 0 through 3), Chandra (LETG+HRC or +ACIS), and XMM-Newton (MOS 1, 2, and pn) by means of evaluating the simultaneous spectra of the BL Lac object PKS 2155−304 observed in 2005, 2006, and 2008. From power-law fits to individual spectra, the photon index agrees among all of the instruments within $\simeq 0.1$. The hydrogen column density is very close to the value assigned to PKS 2155−304 ($= 1.7 \times 10^{20}\,\mathrm{cm}^{-2}$) for the Chandra and XMM-Newton instruments, whose deviation is $\lesssim 1 \times 10^{20}\,\mathrm{cm}^{-2}$, while that of Suzaku bears a larger systematic error of $4 \times 10^{20}\,\mathrm{cm}^{-2}$, at most.

We carried out flux cross-calibration in seven small segments of energy bands between 0.5 keV and 10 keV. In the bands above 2 keV (free from uncertainty of the molecular contamination on the instrument apertures), the Suzaku fluxes are larger than those of XMM-Newton by $\simeq 20\%$, $\simeq 10\%$, and $\lesssim 5\%$ in 2005, 2006, and 2008, respectively, although the 20% difference in 2005 should be regarded as being preliminary because the Suzaku observation in 2005 was carried out with the 1/8 window option. The fluxes of the LETG+HRC in 2006 coincide with those of Suzaku below 2 keV. The fluxes of the LETG+ACIS are compared with those of Suzaku and XMM-Newton with the 2008 data, and are systematically larger than those of Suzaku and XMM-Newton by 10%. These results are compared with the results of the precedent IACHEC paper by Tsujimoto et al. (2011) handling multi-mission data of the compact non-thermal SNR G21.5−0.9. Although some minor differences are found basically within each mission, the results are generally mutually consistent between them.

This research has made use of data obtained from the Chandra Data Archive and the CIAO software package provided by the Chandra X-ray Center (CXC). The authors are deeply grateful to the scheduling and operation teams of Suzaku, XMM-Newton, and Chandra for their effort on having organized and performed the coordinated observation campaign every year since 2005.

References

Anada, T., Dotani, T., Ozaki, M., & Murakami, H. 2008, Proc. SPIE, 7011, 70113X
Anders, E., & Grevesse, N. 1989, Geochim. Cosmochim. Acta, 53, 197
Arnaud, K. A. 1996, ASP Conf. Ser., 101, 17
Bałucińska-Church, M., & McCammon, D. 1992, ApJ, 400, 699
Bamba, A., et al. 2008, PASJ, 60, S153
Beuermann, K., Burwitz, V., & Rauch, T. 2006, A&A, 458, 541
Brinkman, A. C., et al. 1997, Proc. SPIE, 3113, 181
Brinkman, A. C., van Rooijen, J. J., Bleeker, J. A. M., Dijstra, J. H., Heise, J., de Korte, P. A. J., Mewe, R., & Paerels, F. 1987, Astrophys. Lett. Commun., 26, 73
Burke, B. E., Gregory, J. A., Bautz, M. W., Prigozhin, G. Y., Kissel, S. E., Kosicki, B. B., Loomis, A. H., & Young, D. J. 1997, IEEE Trans. Electron Devices, 44, 1633
Dickey, J. M., & Lockman, F. J. 1990, ARA&A, 28, 215
Foschini, L., et al. 2008, A&A, 484, L35
Ishida, M., Okada, S., Hayashi, T., Nakamura, R., Terada, Y., Mukai, K., & Hamaguchi, K. 2009, PASJ, 61, S77
Jansen, F., et al. 2001, A&A, 365, L1
Koyama, K., et al. 2007, PASJ, 59, S23
Mitsuda, K., et al. 2007, PASJ, 59, S1
Murray, S. S., et al. 1997, Proc. SPIE, 3114, 11
Nevalainen, J., David, L., & Guainazzi, M. 2010, A&A, 523, A22
O'dell, S. L., & Weisskopf, M. C. 1998, Proc. SPIE, 3444, 2
Predehl, P., et al. 1997, Proc. SPIE, 3113, 172
Sembay, S., Guainazzi, M., Plucinsky, P., & Nevalainen, J. 2010, AIP Conf. Ser., 1248, 593
Serlemitsos, P. J., et al. 2007, PASJ, 59, S9
Strüder, L., et al. 2001, A&A, 365, L18
Tsujimoto, M., et al. 2011, A&A, 525, A25
Turner, M. J. L., et al. 2001, A&A, 365, L27
Uchiyama, H., et al. 2009, PASJ, 61, S9
Uchiyama, Y., et al. 2008, PASJ, 60, S35
Yamaguchi, H., et al. 2008, PASJ, 60, S141
Yan, M., Sadeghpour, H. R., & Dalgarno, A. 1998, ApJ, 496, 1044